Proc. Schl. Eng. Tokai Univ., Ser. E
39 (2014) 1-6

Numerical Calculation of Current Distribution due to Spark Discharge on Water Surface with Surface Potential as Boundary Condition

by

Nur Shahida MIDI[*1], M.K.A. MUHAMAD[*2] and Ryu-ichiro OHYAMA[*3]

(Received on Mar. 25, 2014 and accepted on May 15, 2014)

Abstract

Numerical calculations of current distribution due to spark discharge on water surface of 0.07 S/m and 5 S/m conductivity were done using two-dimensional axial-symmetry model. In this work, only the water phase is taken into account as the first step to a complete two-phase gas-liquid model. Electric potential on water surface with filamentary discharge length on water surface obtained from laboratory experiments were used as the boundary condition. The calculations were done under both stationary and time-dependent conditions. Result of stationary calculation shows agreement with the maximum values from time-dependent calculation. Comparison with experimental results also had shown a fairly good agreement. The results discussed were the electric field distribution and the current distribution, then in consequently their relation to each other and to the filamentary discharge observed on the water surface during laboratory experiments. It can be concluded that the distribution of electric field and current is influenced by the filamentary discharge.

Keywords: numerical calculation, spark discharge, water surface, current distribution

1. Introduction

Electrical discharge on water surface is being investigated from different perspectives which includes fundamental knowledge which in consequently contributing to various applications in engineering. This includes investigations and applications in water treatment [1-5], maintenance of electrical transmission facilities [6-8] and NOx gases treatment [9]. This electrical phenomenon which includes two dielectrics (water and air) is also being investigated for the interest regarding lightning on water surface [10-12].

With merits such as stronger winds and spacious open area that will eliminate the visual and noise impact, wind turbines are widely being built at the sea area [13]. Despite that, due to their height of over 100 meters, the wind turbines are exposed to hazards due to direct and indirect lightning [14]. As access to offshore sites for maintenance and repairs is an important aspect for cost reducing, lightning protection in the sea area has become a major issue. This also applies to other objects on sea such as boats [15], offshore photovoltaic facility [16], and also human [17]. For that matter, an understanding regarding lightning phenomenon on water surface is crucial, where various parameters are ought to be considered.

Laboratory-scale electrode system imitating lightning phenomenon on water surface using spark discharge [18] had showed that the conductivity of water is influencing the discharge occurred on water surface and also the current distribution. However, there is limitation in experimental investigations such as the apparatus scale, and for this, computer-aided simulation is the tool to assist the investigation.

In this work, numerical calculations of current distribution due to spark discharge on water surface with different conductivity were done. As this phenomenon includes both air and water phase, it is very crucial that the calculation takes account the discharge phenomenon at the air phase which includes a voltage drop at the air gap, then in consequently the discharge and current conduction phenomena at the water phase.

As the first step of this work, this paper is focusing on the discharge and conduction phenomena at the water phase. In this paper, calculation of current distribution using

*1 Graduate Student, Course of Science and Technology
*2 Graduate Student, Course of Electrical and Electronic System
*3 Professor, Department of Electrical and Electronic Engineering

experimentally measured water surface potential as the boundary condition is discussed. The calculations were done under both stationary and time-dependent condition, and the results are then compared with the experimental results.

2. Calculation model and boundary condition

In our previous work, an electrode system as shown in Fig. 1 was developed to observe the current distribution due to spark discharge on water surface of different conductivity, σ; varied using tap water and saline solutions. The electrode system is consisted of a discharge electrode, which is placed with an air gap from the water surface; and 9 underwater grounding electrodes to observe the underwater current distribution. 25 kV of impulse lightning (1.2/50μs) was applied to the discharge electrode to generate the spark discharge at the air gap. The number 1.2/50μs indicates that 1.2μs are needed for the surge to reach its peak value (duration of wave front), and 50μs are taken for the surge to decay from the peak to its 50% value (duration of wave tail). From the experiments, a significant difference was obtained between tap water and saline solutions. During the discharge process, filamentary discharge sprouting on the water surface had been observed as shown in Fig. 2, where (a) is for tap water (σ = 0.07 S/m) and (b) is for saline solution with the same σ as seawater (σ = 5 S/m). All other saline solutions had shown similar characteristics to 5 S/m even with a small difference of σ to tap water [18].

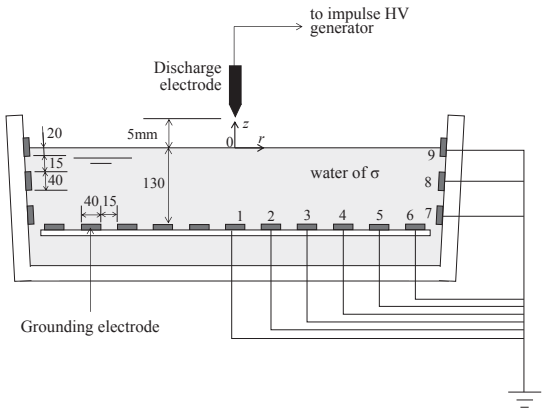

Fig. 1 Cross sectional view of electrode system for observing discharge current distribution.

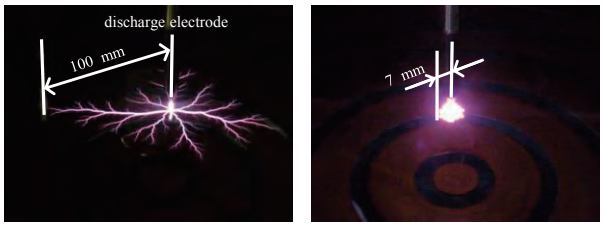

(a) 0.07 S/m (b) 5 S/m

Fig. 2 Filamentary discharge on water surface.

On that matter, only the calculation for tap water (σ = 0.07 S/m) and saline solution with the same conductivity to seawater (σ = 5 S/m) are done in this work. The calculation model used in this work is as shown in Fig. 3 which is a two-dimensional axial-symmetry model. The mesh is consisted of 12634 triangular elements with finer elements at the boundaries which are representing the water surface and ground. Electric potential at the water surface, $V_{surface}$ is the experimentally measured electric potential as shown in Fig. 4, which was obtained from the peak values of the electric potential waveforms, where r is the distance from the discharge point. These electric potential were obtained using

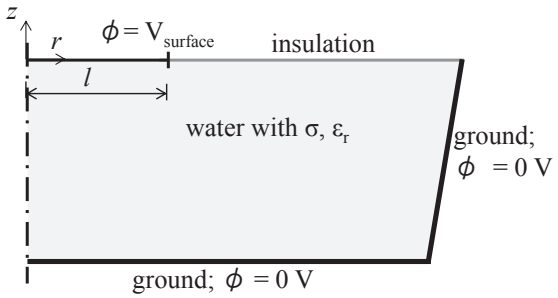

Fig. 3 Calculation model.

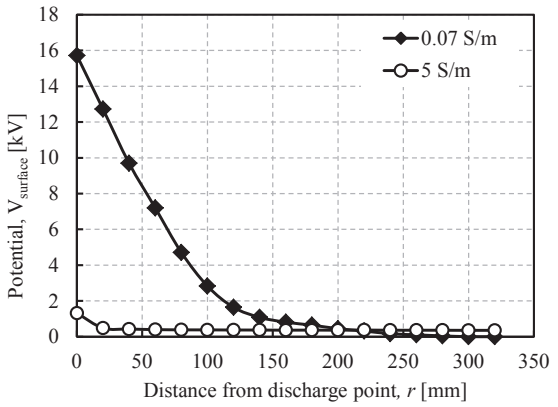

Fig. 4 Peak values of water surface potential, $V_{surface}$ measured in experiments for stationary calculation.

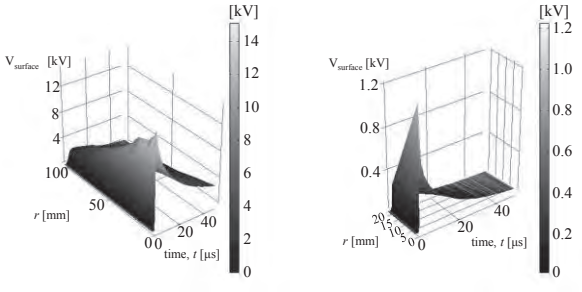

(a) 0.07 S/m (b) 5 S/m

Fig. 5 Waveforms of $V_{surface}$ at different r for time-dependent calculation.

a tungsten-tipped measurement probe placed perpendicularly to the water surface, and the tip was in contact with the water surface[18]. The measurement was done in a 20 mm interval. $V_{surface}$ with both r and time, t as the agreement for time-dependent calculation is shown in Fig. 5. Maximum r values for $V_{surface}$ used in the calculation are according to the l values which were determined from the filamentary discharge length as in Fig. 2 and are different for tap water and seawater. For seawater, although only 7 mm of filamentary discharge was observed, the l value was set to 20 mm; which is the second value of electric potential measured after the electric potential at r = 0 mm, V_{0mm} as can be seen in Fig. 4. Insulation in the model means that no electric current flows into the boundary where $\mathbf{n} \cdot \mathbf{J} = 0$, with $\mathbf{n}$ direction is perpendicular to the water surface. This is equivalent to where no filamentary discharges were observed on the water surface during the experiments. The parameters used in the calculation which includes the dielectric properties of tap water and seawater are provided in Table 1.

The electric field and current were calculated by employing the equations below, where $\mathbf{J}$: current density [A/m^2], $\mathbf{E}$: electric field [V/m], ø : electric potential [V], and $\mathbf{D}$: electric displacement field [C/m^2] using the AC/DC module of Comsol Multiphysics. Eq. (2-1) is for stationary calculation while eq. (2-2) is for time-dependent calculation.

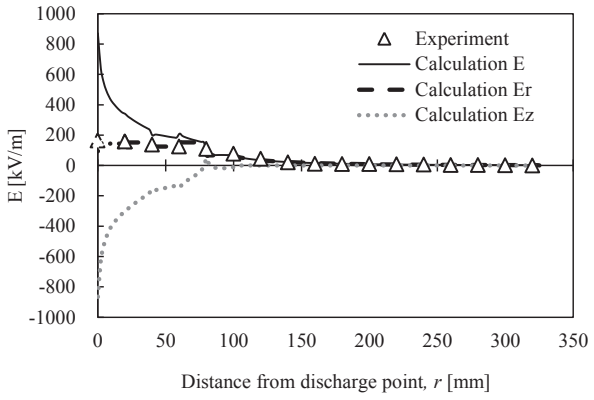

(a) 0.07 S/m

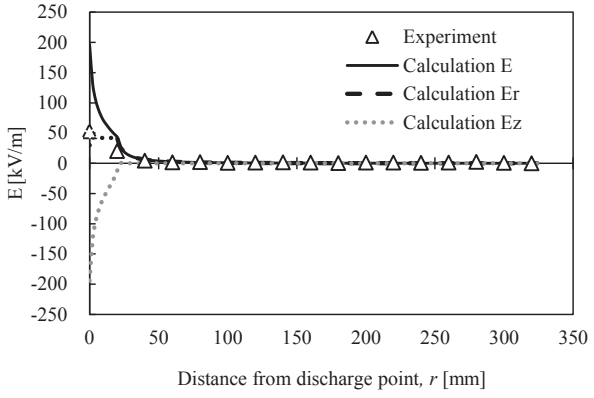

(b) 5 S/m

Fig. 6 Electric field component on water surface (z = 0 mm) obtained from stationary calculation.

The calculations were done under both stationary and time-dependent condition, although the spark discharge is a transient phenomenon which automatically suggests that only a time-dependent calculation is needed. A stationary calculation is also important as a quick spatial evaluation of the electrical properties involved.

$$\mathbf{E} = -\nabla ø \qquad (1)$$

$$\mathbf{J} = \sigma \mathbf{E} \qquad (2\text{-}1)$$

$$\mathbf{J} = \sigma \mathbf{E} + \frac{\partial \mathbf{D}}{\partial t} \qquad (2\text{-}2)$$

Table 1 Calculation parameters

Property	tap water	seawater
Conductivity, σ[S/m]	0.07	5
Relative permittivity, ε_r	78.5	68.3
Boundary length, l [mm]	100	20

3. Results and discussion

Fig. 6 shows the electric field components E_r (r-component), E_z (z-component) and E on water surface (z = 0 mm) obtained from stationary calculation. The calculation result of E_r shows a fairly good agreement with the experimental result. The experimental result of E_r on water surface was obtained

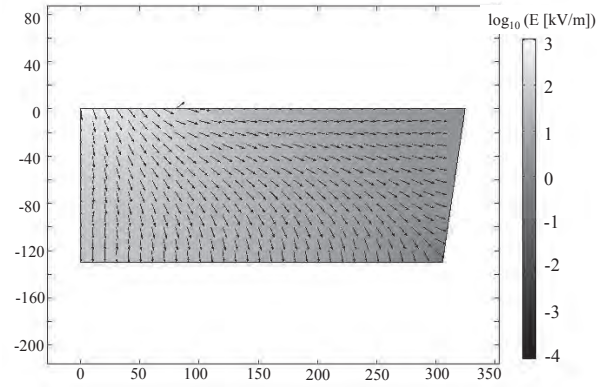

(a) 0.07 S/m

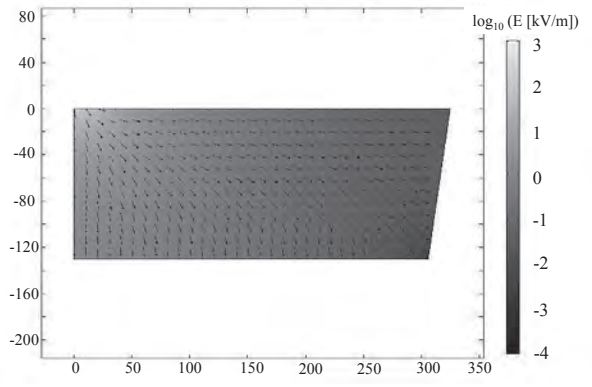

(b) 5 S/m

Fig. 7 Electric field obtained from stationary calculation. (arrows : electric field vectors; color map : electric field magnitude in log scale, $\log_{10}$ (V[kV/m]))

from the differential of $V_{surface}$ in r direction. As the potential matrix for differential in z direction could not be obtained with the same measurement method, the comparisons for E_z and E are not available. From this figure, it can be seen that at the positions where $r < l$ (which represent the filamentary discharge on water surface), the electric field are mainly consisted of E_z. At the position where $r > l$, the electric field are mainly consisted of E_r. This is confirmed by the arrows which represent the electric field vectors in Fig. 7. For the symmetry axis (r = 0 mm), where the arrows are mostly pointing downwards, the electric field is mostly consisted of E_z, where E_r is almost zero. From these results, it can be concluded that the filamentary discharge on water surface (or $V_{surface}$ in the model) is influencing the electric field distribution.

The distribution of electric field to underwater expressed by both the vectors arrows and the color map in log scale ($\log_{10}$ E [kV/m]) suggest that the area which are affected by the filamentary discharge is different for both conductivity. The E for 0.07 S/m is more affected than 5 S/m, considering the longer l of 0.07S/m. For time-dependent calculation, similar distributions are obtained which the magnitude of E decrease with the increase in time.

The electric field distribution relation with time is shown in Fig. 8, obtained from the time-dependent calculation. A difference to the stationary calculation result in the electric field magnitude of 0.07 S/m can be observed. This is caused by the time-dependent waveform of 0.07 S/m (Fig. 5(a)) which did not show a smooth decrease of $V_{surface}$ with the increase in r, compared to 5 S/m (Fig. 5(b)) which shows a smooth waveform resulting to less obvious difference of E between stationary and time-dependent calculation results.

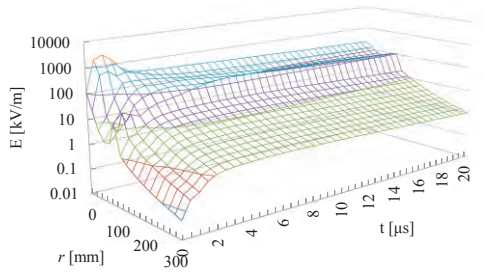

(a) 0.07 S/m

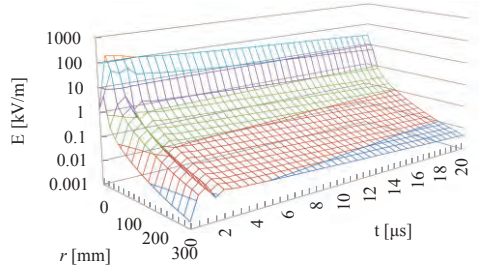

(b) 5 S/m

Fig. 8 Electric field as a function of r and time obtained from time-dependent calculation.

Fig. 9 shows the current distribution obtained from stationary calculation where the lines are the current vectors while the color map is the current density magnitude in log scale ($\log_{10}$ I [A/m^2]). Similar to the electric field distribution, the distribution of discharge current is also influenced by the filamentary discharge. It can be seen that the lines are mainly originating from the position where boundary condition is added which is identical to the vectors of E as in Fig. 7. Besides that, it can be seen that the current lines at around 100 mm for 0.07 S/m and 20 mm for 5 S/m are denser compared to other area. Denser current streamlines indicate higher magnitude of the current. This is coherent with results obtained by Matsuo et al. which states that most of the discharge current flows from the tip part of the local discharge regardless of the propagation length [7]. Similar with the case of electric field in Fig.6, the time-dependent current distributions resemble the stationary calculation result in which the magnitude decreases with the increase in time.

Fig. 10 shows the discharge current waveforms at the grounding electrodes obtained from the time-dependent

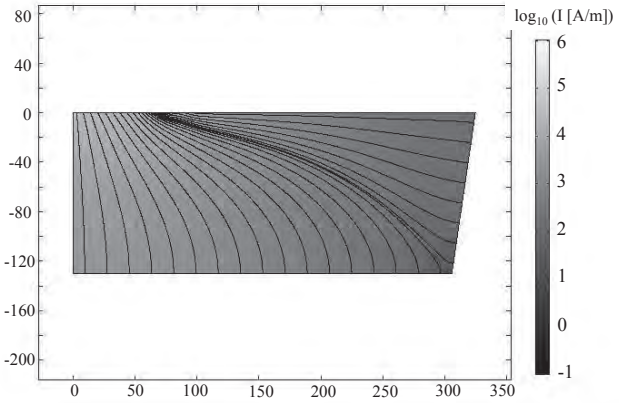

(a) 0.07 S/m

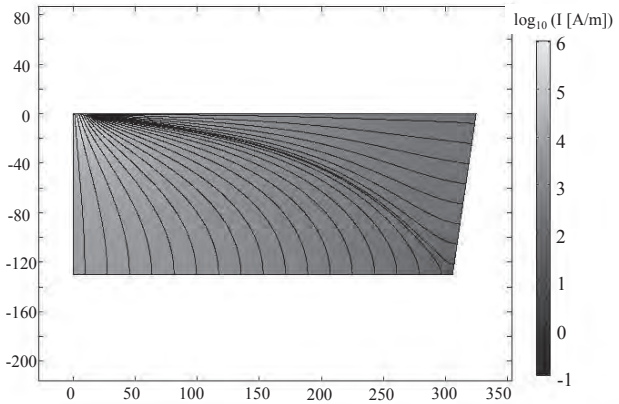

(b) 5 S/m

Fig. 9 Current distribution obtained from stationary calculation. (lines : current vectors; color map : current density magnitude in log scale, $\log_{10}$ (I [A/m^2]))

calculation. These waveforms resemble the current waveforms that were obtained from the experiments [18]. As the calculation model in this work is only considering the water phase (instead of the water and air two-phase discharge phenomenon of the electrode system), it can be concluded these current waveform is not directly affected by the current at the discharge electrode (which is at the air phase), or in other words, the $V_{surface}$ is enough to obtain the waveforms.

Fig. 11 shows the discharge current distribution at the grounding electrodes for both stationary and time-dependent calculation with comparison to the experimental values. The current density values for time-dependent were obtained from the highest value of the current density calculated, which is equal to the peaks of waveforms in Fig. 10. Note that the times for the highest value to occur are different according to the electrode number especially for 0.07 S/m. This also applies to the experimental values that were obtained from the current waveform's peak, where a time lag is observed as the grounding electrode number shifted from 1 to 9. From these figures, it can be seen that the stationary calculation results agree well with the peak values for time-dependent calculations in term of the distribution pattern. The slight difference between the two calculation values is considered due to the effect of electric displacement field **D** [C/m^2], as suggested by Eq. 2-1 and Eq. 2-2. For 0.07 S/m, the

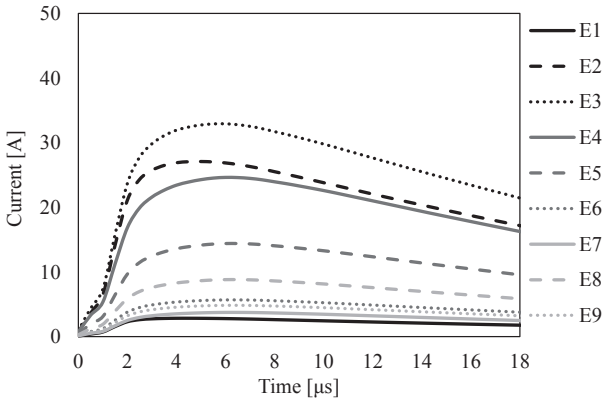

(a) 0.07 S/m

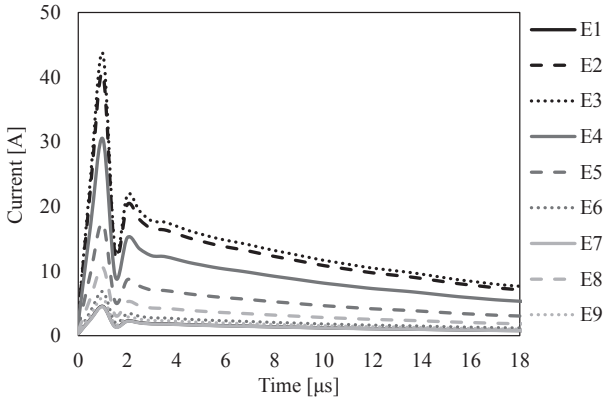

(b) 5 S/m

Fig. 10 Current waveforms at the grounding electrodes obtained from time- dependent calculation.

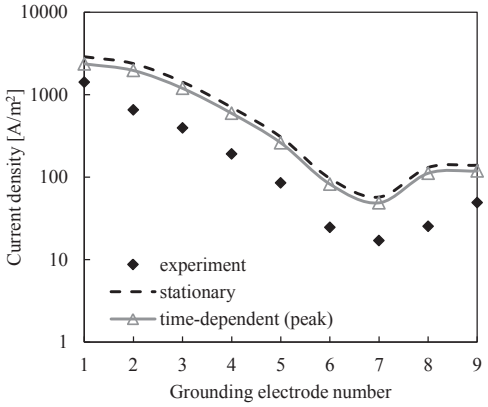

(a) 0.07 S/m

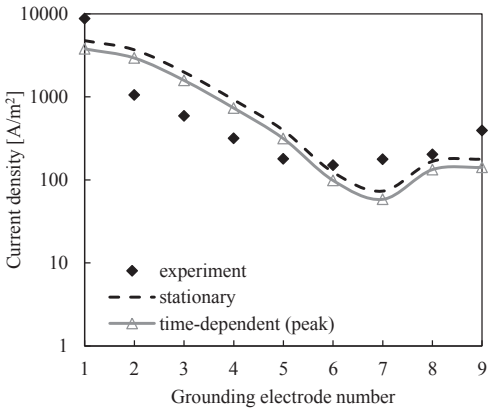

(b) 5 S/m

Fig. 11 Current distribution at the grounding electrodes.

time-dependent calculation results are 15% smaller than that of stationary calculation results. On the other hand, a difference of 20% was observed. The 5% difference between the two conductivities is considered to be caused by the difference in E as in Fig. 6 and Fig. 8. It also can be seen that the calculated discharge current shows the same pattern to the experimental results. However, there is differences not more than one power order in the current density values. This might be caused by the influence of electric fields generated by the residual space charge, which accentuated or weakened the total electric field during the experiments.

From these results, it can be concluded that for a water phase model, boundary condition of electric potential considering the filamentary discharge on water surface is appropriate for the calculation of current distribution to underwater. From the electric field vectors and current streamlines, the significance of $V_{surface}$ (or filamentary discharge on water surface) towards the two fields can be seen.

4. Concluding remark

Calculation of current distribution to underwater due to spark discharge on water surface is done with a single water

phase calculation model. From the calculation results, the relation between surface potential, electric field and current distribution was identified. From this, the relation between filamentary discharge on water surface and current distribution to underwater observed during the experiments is established. The results that could not be obtained from the experiments such as the electric field and current vectors are made available by this numerical calculation. The reliability is confirmed by the comparison with experimental values that shows a relatively fair agreement. On the whole, it can be concluded that in calculation of current distribution to underwater using electric potential on water surface as the boundary condition, considering only the potential at the filamentary part is adequate.

Although this calculation using electric potential on water surface is considered enough to simulate the current distribution underwater, it is still reasonable for a demand of calculation model considering both the air and water phase. This is because development of a complete two phase calculation model will reduce the needs in physical experiments, where the needs to measure surface potential can be eliminated. This one phase calculation result will be the initial step for the calculation considering both the air and water phase. Subsequently, a numerical calculation that is including the voltage drop at the air phase above the water surface is to be considered.

Acknowledgment

The first author would like to thank the International Islamic University Malaysia (IIUM) and Ministry of Education (MoE) Malaysia for a graduate fellowship to support her PhD course.

References

1) M. Sato, T. Tokutate, T. Ohshima, and A.T. Sugiarto : Aqueous Phenol Decomposition by Pulsed Discharge on the Water Surface, IEEE Trans. Ind. Appl. **44**-5 (1998) pp. 1397-1402.
2) J.A. Robinson, M.A. Bergougnou, W.L. Cairns, G.S. Peter Castle, and I.I. Inculet : A New Type of Ozone Generator using Taylor Cones on Water Surfaces, IEEE Trans. Ind. Appl. **34**-6 (1998), pp. 1218-1224.
3) M. Sato, A.T. Sugiarto, T. Tokutate, and T. Ohshima : Developing Water Surface Discharge for Wastewater Treatment, Instrumentasi **28**-1, (2004) pp. 6-10.
4) P. Lukes, A.T. Appleton, and B.R. Locke : Hydrogen Peroxide and Ozone Formation in Hybrid Gas-Liquid Electrical Discharge Reactors, IEEE Trans. Ind. Appl. **40**-1 (2004) pp. 60-67.
5) P. Bruggeman, E. Ribežl, J. Degroote, J. Vierendeels, and C. Leys : Plasma Characteristics and Electrical Breakdown between Metal and Water Electrodes, J. Optoelectron. Adv. M. **10**-8 (2008) pp. 1964-1967.
6) Y. Nakao, H. Itoh, Y. Sakai, and H. Tagashira : Studies of the Creepage Discharge on Surface of Liquids, IEEE Trans. Electr. Insul. **23**-4, (1988) pp. 677-687.
7) H. Matsuo, T. Yamashita, and T. Fujishima : Shape of Contacting Surface between an Electrolytic Solution and Local Discharge on it, IEEE Trans. Dielectr. Electr. Insul. **10**-4 (2003) pp. 634-640.
8) H. Matsuo, T. Yamashita, T. Fujishima, H. Oniki, and K. Kawamura : Electric Potential near a Tip of a Local Discharge on an Electrolytic Solution, IEEJ Trans. Fundamental and Materials, **124**-7 (2004) pp. 541-546.
9) T. Fujii and M. Rea, "Treatment of NOx in Exhaust Gas by Corona Plasma over Water Surface : Vacuum **59** (2000) pp. 228-235.
10) K.I. Selin and H. Ryzko : Electric Discharges above a Water Surface at Positive Impulse Discharge, Proc. IEEE Southeast-Con. Reg. 3 Conf. (1973) pp. U.6.1-U.6.5.
11) A.M. Anpilov, É.M. Barkhudarov, V.A. Kop'ev, and I.A. Kossyi : Atmospheric Electric Discharge into Water, Plasma Phys. Rep. **32**-11 (2006) pp. 968-972.
12) D. Okano : Impedance Property of Lightning Impulse Discharge in Short Composite Gap Consisting of Air and Water, 2012 Int. Conf. Lightning Protection (2012) pp. 1-5.
13) S-P. Breton and G. Moe : Status, Plans and Technologies for Offshore Wind Turbines in Europe and North America, Renewable Energy, **34** (2009) pp. 646-654.
14) ABB Lightning Protection Group, Lightning and Overvoltage Protection : Wind Turbines, France, 2007
15) E.M. Thomson : A Critical Assessment of the U.S. Code for Lightning Protection of Boats, IEEE Trans. Electromn. Compat. **33**-2 (1991) pp. 132-138.
16) K. Trapani and D.L. Millar : Proposing Offshore Photovoltaic (PV) Technology to the Energy Mix of the Maltese Islands, Energy Conversion and Management **67** (2013) pp. 18-26.
17) J. Wiater : Electric Shock Hazard Limitation in Water during Lightning Strikes, Electrical Review (2012) pp. 52-53.
18) N.S. Midi and R. Ohyama : Underwater Current Distribution Induced by Spark Discharge on a Water Surface, J. Electrostat. **71**-4 (2013) pp. 823-828.